Ladder-Type Oligo-*p*-phenylene-Containing Copolymers with High Open-Circuit Voltages and Ambient Photovoltaic Activity

Qingdong Zheng, Byung Jun Jung, Jia Sun, and Howard E. Katz*

Department of Materials Science and Engineering and Department of Chemistry, The Johns Hopkins University, 102 Maryland Hall, 3400 North Charles Street, Baltimore, Maryland 21218

Received October 29, 2009; E-mail: hekatz@jhu.edu

Abstract: Four ladder-type oligo-*p*-phenylene containing donor−acceptor copolymers were designed, synthesized, and characterized. The ladder-type oligo-*p*-phenylene was used as an electron donor unit in these copolymers to provide a deeper highest occupied molecular orbital (HOMO) level for obtaining polymer solar cells with a higher open-circuit voltage, while 4,7-dithien-2-yl-2,1,3-benzothiadiazole or 5,8-dithien-2-yl-2,3-diphenylquinoxaline was chosen as an electron acceptor unit to tune the electronic band gaps of the polymers for a better light harvesting ability. These copolymers exhibit field-effect mobilities as high as 0.011 cm^2/(V s). Compared to fluorene containing copolymers with the same acceptor unit, these ladder-type oligo-*p*-phenylene containing copolymers have enhanced and bathochromically shifted absorption bands and much better solubility in organic solvents. Photovoltaic applications of these polymers as light-harvesting and hole-conducting materials are investigated in conjunction with [6,6]-phenyl-C61-butyric acid methyl ester (PC$_{61}$BM) or [6,6]-phenyl-C71-butyric acid methyl ester (PC$_{71}$BM). Without extensive optimization work, a power conversion efficiency (PCE) of 3.7% and a high open-circuit voltage of 1.06 V are obtained under simulated solar light AM 1.5 G (100 mW/cm^2) from a solar cell with an active layer containing 20 wt % ladder-type tetra-*p*-phenylene containing copolymer (**P3FTBT6**) and 80 wt % PC$_{61}$BM. Moreover, a high PCE of 4.5% was also achieved from a solar cell with an active layer containing 20 wt % **P3FTBT6** and 80 wt % PC$_{71}$BM.

---

1. Introduction

In the past decade, there has been increasing interest in polymer solar cells due to the growing demand for "green" and sustainable energy. Compared to today's inorganic solar cells, conjugated polymer-based solar cells are expected to be cheaper because they can be fabricated at a much lower cost with the aid of large area solution casting or roll-to-roll manufacturing of flexible modules.[1−3] Since the introduction of the bulk heterojunction (BHJ) concept,[4] regioregular poly(3-hexyl-thiophene) (P3HT) has been chosen as the standard electron donor material in polymer BHJ solar cells. The highest power conversion efficiency reported for the polymer blend of P3HT and [6,6]-phenyl C61 butyric acid methyl ester (PC$_{61}$BM, or PCBM) is ∼5%.[5−10] It is well-known that the power conversion efficiency and fill factor of a solar cell device are calculated according to the following equations:

$$\eta = (FF \times J_{sc} \times V_{oc})/P_{in} \tag{1}$$

$$FF = (J_{max} \times V_{max})/(J_{sc} \times V_{oc}) \tag{2}$$

where P_{in} is the input power; J_{sc} and V_{oc} are the short-circuit current and open-circuit voltage, respectively; J_{max} and V_{max} are the current density and voltage at the maximum power output; and *FF* is the fill factor. In-depth investigation of the solar cell devices based on the P3HT:PCBM system reveals that its efficiency is limited by low open-circuit voltage V_{oc} (∼0.6 V) and the relatively large band gap of P3HT which limits its harvesting ability (low J_{sc}). Therefore, in recent years many low band gap polymers have been developed to increase the light absorbing ability of solar cell devices,[11−21] because the light

(1) Coakley, K. M.; McGehee, M. D. *Chem. Mater.* **2004**, *16*, 4533–4542.
(2) Chen, L. M.; Hong, Z. R.; Li, G.; Yang, Y. *Adv. Mater.* **2009**, *21*, 1434–1449.
(3) Gunes, S.; Neugebauer, H.; Sariciftci, N. S. *Chem. Rev.* **2006**, *107*, 1324–1338.
(4) Sariciftci, N. S.; Smilowitz, L.; Heeger, A. J.; Wudl, F. *Science* **1992**, *258*, 1474–1476.
(5) Campoy-Quiles, M.; Ferenczi, T.; Agostinelli, T.; Etchegoin, P. G.; Kim, Y.; Anthopoulos, T. D.; Stavrinou, P. N.; Bradley, D. D. C.; Nelson, J. *Nat. Mater.* **2008**, *7*, 158–164.
(6) Li, G.; Yao, Y.; Yang, H.; Shrotriya, V.; Yang, G.; Yang, Y. *Adv. Funct. Mater.* **2007**, *17*, 1636–1644.
(7) Li, G.; Shrotriya, V.; Huang, J.; Yao, Y.; Moriarty, T.; Emery, K.; Yang, Y. *Nat. Mater.* **2005**, *4*, 864–868.
(8) Wang, W.; Wu, H.; Yang, C.; Luo, C.; Zhang, Y.; Chen, J.; Cao, Y. *Appl. Phys. Lett.* **2007**, *90* (18), 183512/1–183512/3.
(9) Ma, W.; Yang, C.; Gong, X.; Lee, K.; Heeger, A. J. *Adv. Funct. Mater.* **2005**, *15*, 1617–1622.
(10) Woo, C. H.; Thompson, B. C.; Kim, B. J.; Toney, M. F.; Frechet, J. M. J. *J. Am. Chem. Soc.* **2008**, *130*, 16324–16329.
(11) Hou, J.; Chen, H.-Y.; Zhang, S.; Li, G.; Yang, Y. *J. Am. Chem. Soc.* **2008**, *130*, 16144–16145.
(12) Liang, Y. Y.; Wu, Y.; Feng, D. Q.; Tsai, S. T.; Son, H. J.; Li, G.; Yu, L. P. *J. Am. Chem. Soc.* **2009**, *131*, 56–57.
(13) Baek, N. S.; Hau, S. K.; Yip, H. L.; Acton, O.; Chen, K. S.; Jen, A. K. Y. *Chem. Mater.* **2008**, *20*, 5734–5736.
(14) Chen, C.-P.; Chan, S.-H.; Chao, T.-C.; Ting, C.; Ko, B.-T. *J. Am. Chem. Soc.* **2008**, *130*, 12828–12833.
(15) Lee, J. K.; Ma, W. L.; Brabec, C. J.; Yuen, J.; Moon, J. S.; Kim, J. Y.; Lee, K.; Bazan, G. C.; Heeger, A. J. *J. Am. Chem. Soc.* **2008**, *130*, 3619–3623.
(16) Lee, J.-Y.; Shin, W.-S.; Haw, J.-R.; Moon, D.-K. *J. Mater. Chem.* **2009**, *19*, 4938–4945.

absorbing ability is directly related to the value of short-circuit current J_{sc}. However, the open-circuit voltages for most of these low band gap polymer-based solar cells are in the range 0.35−0.80 V.[11−13,15,18,21] It has been reported that there is a correlation between V_{oc} and the difference between the highest occupied molecular orbital (HOMO) of the donor and the lowest unoccupied molecular orbital (LUMO) of the acceptor used in bulk heterojunction (BHJ) solar cells. Therefore, reduction of the band gap of a donor polymer will also reduce the open-circuit voltage, because of a decreased energy difference between the HOMO of a polymer and the LUMO of an acceptor (e.g., $PC_{61}BM$).

To achieve a polymer solar cell device with a high light harvesting ability (low band gap) as well as a high open-circuit voltage, one feasible approach is to design alternating donor−acceptor copolymers, where the electron donor unit may provide a deeper HOMO level and the electron acceptor unit is used to tune the electronic band gap of the polymers. Recently, this kind of donor−acceptor polymer has been successfully used for high performance solar cells by choosing fluorene or carbazole as the electron donor and benzothiadiazole, quinoxaline, or thienopyrazine as the electron acceptor.[22−32]

The structure of ladder-type oligo-*p*-phenylenes consists of several "linearly overlapping" fluorenes, and it would serve as a good electronic donor owing to its extended π-conjugation. The extended π-conjugation of ladder-type oligo-*p*-phenylene derivatives may lead to a broader, more intense absorption band

compared to fluorene derivatives and, thus, result in an enhanced solar light harvesting. At the same time, for every repeat unit in the ladder-type oligo-*p*-phenylene containing polymers, there are at least four alkyl chains on the polymer backbone. Solubilizing alkyl chains can be easily introduced into this unique molecular backbone, which may provide a better solution processability of the target polymers. As a result, indenofluorene or ladder-type oligo-*p*-phenylene has been chosen as a building block for materials with various applications.[33−38] However, to the best of our knowledge, there is no work on the ladder-type oligo-*p*-phenylene containing copolymers for photovoltaic (PV) applications. In this work, we choose ladder-type oligo-*p*-phenylenes as electron donor building blocks and 4,7-dithien-2-yl-2,1,3-benzothiadiazole or 5,8-dithien-2-yl-2,3-diphenylquinoxaline as an electron acceptor building block to obtain copolymers with deeper HOMO energy levels, broader spectral absorption ranges, and improved phase separation properties with PCBMs. Among polymers for PV applications, the hexyl group has a good balance between crystallinity and miscibility in the bid to achieve optimal morphology. On the other hand, polymers with decyl groups have better solubility compared to those with hexyl groups,[39] and the decyl group was reported to be a good side chain for fluorene-containing polymers to achieve high power conversion efficiency.[28] Therefore, in this work, both hexyl and decyl are chosen as side chains for targeted soluble copolymers. We report on the synthesis, characterization, photophysical properties, field effect transistor behaviors, and photovoltaic properties of these ladder-type oligo-*p*-phenylene containing copolymers.

2. Results and Discussion

2.1. Synthesis and Characterization. The syntheses of the four new copolymers are shown in Scheme 1. They were prepared by a palladium-catalyzed Suzuki coupling reaction between 4,7-bis(5-bromo-2-thienyl)-2,1,3-benzothiadiazole (**3**) or 5,8-bis-(5-bromothiophen-2-yl)-2,3-diphenylquinoxaline (**4**), and three diboronated ladder-type oligo-*p*-phenylenes (**1a−b**, **2**). For each copolymer, an end-capping reaction was performed using bromobenzene and phenyl boronic acid to increase the stability of the polymer. The synthesis of monomers **1a−b** and **2** is outlined in Scheme 2. As shown in Scheme 2, the preparation of comonomers **1a−b** started from compounds **5a−b**, which were selectively brominated at the 2- and 8-positions, with copper(II) bromide on an aluminum oxide matrix in carbon tetrachloride affording 2,8-dibromo-6,6′,12,12′-tetraalkyl-6,12-dihydroindeno-[1,2*b*]fluorene (**6a−b**). Then compounds **6a−b** were reacted with 4,4,4′,4′,5,5,5′,5′-octamethyl-2,2′-bi(1,3,2-dioxaborolane) to yield compounds **1a−b** with the

(17) Moule, A. J.; Tsami, A.; Bunnagel, T. W.; Forster, M.; Kronenberg, N. M.; Scharber, M.; Koppe, M.; Morana, M.; Brabec, C. J.; Meerholz, K.; Scherf, U. *Chem. Mater.* **2008**, *20*, 4045−4050.

(18) Muhlbacher, D.; Scharber, M.; Morana, M.; Zhu, Z. G.; Waller, D.; Gaudiana, R.; Brabec, C. *Adv. Mater.* **2006**, *18*, 2884−2889.

(19) Zhang, F. L.; Mammo, W.; Andersson, L. M.; Admassie, S.; Andersson, M. R.; Inganas, L.; Admassie, S.; Andersson, M. R.; Ingands, O. *Adv. Mater.* **2006**, *18*, 2169−2173.

(20) Zhang, F. L.; Perzon, E.; Wang, X. J.; Mammo, W.; Andersson, M. R.; Inganas, O. *Adv. Funct. Mater.* **2005**, *15*, 745−750.

(21) Mondal, R.; Miyaki, N.; Becerril, H. A.; Norton, J. E.; Parmer, J.; Mayer, A. C.; Tang, M. L.; Bredas, J.-L.; McGehee, M. D.; Bao, Z. *Chem. Mater.* **2009**, *21*, 3618−3628.

(22) Svensson, M.; Zhang, F. L.; Veenstra, S. C.; Verhees, W. J. H.; Hummelen, J. C.; Kroon, J. M.; Inganas, O.; Andersson, M. R. *Adv. Mater.* **2003**, *15*, 988−991.

(23) Hou, Q.; Zhou, Q.; Zheng, L.; Deng, X.; Yu, G.; Cao, Y. *Appl. Phys. Lett.* **2004**, *84*, 1653−1655.

(24) Zhang, F. L.; Jespersen, K. G.; Bjorstrom, C.; Svensson, M.; Andersson, M. R.; Sundstrom, V.; Magnusson, K.; Moons, E.; Yartsev, A.; Inganas, O. *Adv. Funct. Mater.* **2006**, *16*, 667−674.

(25) Gadisa, A.; Zhang, F. L.; Sharma, D.; Svensson, M.; Andersson, M. R.; Inganas, O. *Thin Solid Films* **2007**, *515*, 3126−3131.

(26) Gedefaw, D.; Zhou, Y.; Hellstroem, S.; Lindgren, L.; Andersson, L. M.; Zhang, F.; Mammo, W.; Inganaes, O.; Andersson, M. R. *J. Mater. Chem.* **2009**, *19*, 5359−5363.

(27) Slooff, L. H.; Veenstra, S. C.; Kroon, J. M.; Moet, D. J. D.; Sweelssen, J.; Koetse, M. M. *Appl. Phys. Lett.* **2007**, *90*, 143506/1−143506/3.

(28) Veldman, D.; Ipek, O.; Meskers, S. C. J.; Sweelssen, J.; Koetse, M. M.; Veenstra, S. C.; Kroon, J. M.; Bavel, S. S. v.; Loos, J.; Janssen, R. A. J. *J. Am. Chem. Soc.* **2008**, *130*, 7721−7735.

(29) (a) Blouin, N.; Michaud, A.; Gendron, D.; Wakim, S.; Blair, E.; Neagu-Plesu, R.; Belletete, M.; Durocher, G.; Tao, Y.; Leclerc, M. *J. Am. Chem. Soc.* **2007**, *130*, 732−742. (b) Blouin, N.; Michaud, A.; Leclerc, M. *Adv. Mater.* **2007**, *19*, 2295−2300.

(30) Wen, S.; Pei, J.; Zhou, Y.; Li, P.; Xue, L.; Li, Y.; Xu, B.; Tian, W. *Macromolecules* **2009**, *42* (14), 4977−4984.

(31) Park, S. H.; Roy, A.; Beaupre, S.; Cho, S.; Coates, N.; Moon, J. S.; Moses, D.; Leclerc, M.; Lee, K.; Heeger, A. J. *Nat. Photonics* **2009**, *3*, 297−302.

(32) (a) Lindgren, L. J.; Zhang, F.; Andersson, M.; Barrau, S.; Hellstroem, S.; Mammo, W.; Perzon, E.; Inganaes, O.; Andersson, M. R. *Chem. Mater.* **2009**, *21*, 3491−3502. (b) Kitazawa, D.; Watanabe, N.; Yamamoto, S.; Tsukamoto, J. *Appl. Phys. Lett.* **2009**, *95* (5), 053701/1−053701/3.

(33) Setayesh, S.; Marsitzky, D.; Mullen, K. *Macromolecules* **2000**, *33*, 2016−2020.

(34) Sonar, P.; Zhang, J.; Grimsdale, A. C.; Mullen, K.; Surin, M.; Lazzaroni, R.; Leclere, P.; Tierney, S.; Heeney, M.; McCulloch, I. *Macromolecules* **2004**, *37*, 709−715.

(35) Zheng, Q.; Gupta, S. K.; He, G. S.; Tan, L.-S.; Prasad, P. N. *Adv. Funct. Mater.* **2008**, *18*, 2770−2779.

(36) Usta, H.; Risko, C.; Wang, Z.; Huang, H.; Deliomeroglu, M. K.; Zhukhovitskiy, A.; Facchetti, A.; Marks, T. J. *J. Am. Chem. Soc.* **2009**, *131*, 5586−5608.

(37) Zhang, W.; Smith, J.; Hamilton, R.; Heeney, M.; Kirkpatrick, J.; Song, K.; Watkins, S. E.; Anthopoulos, T.; McCulloch, I. *J. Am. Chem. Soc.* **2009**, *131*, 10814−10815.

(38) Yen, W.-C.; Pal, B.; Yang, J.-S.; Hung, Y.-C.; Lin, S.-T.; Chao, C.-Y.; Su, W.-F. *J. Polym. Sci., Part A: Polym. Chem.* **2009**, *47*, 5044−5056.

(39) Nguyen, L. H.; Hoppe, H.; Erb, T.; Guenes, S.; Gobsch, G.; Sariciftci, N. S. *Adv. Funct. Mater.* **2007**, *17*, 1071−1078.

Scheme 1. Synthesis of Ladder-Type Oligo-*p*-phenylene-Containing Copolymers
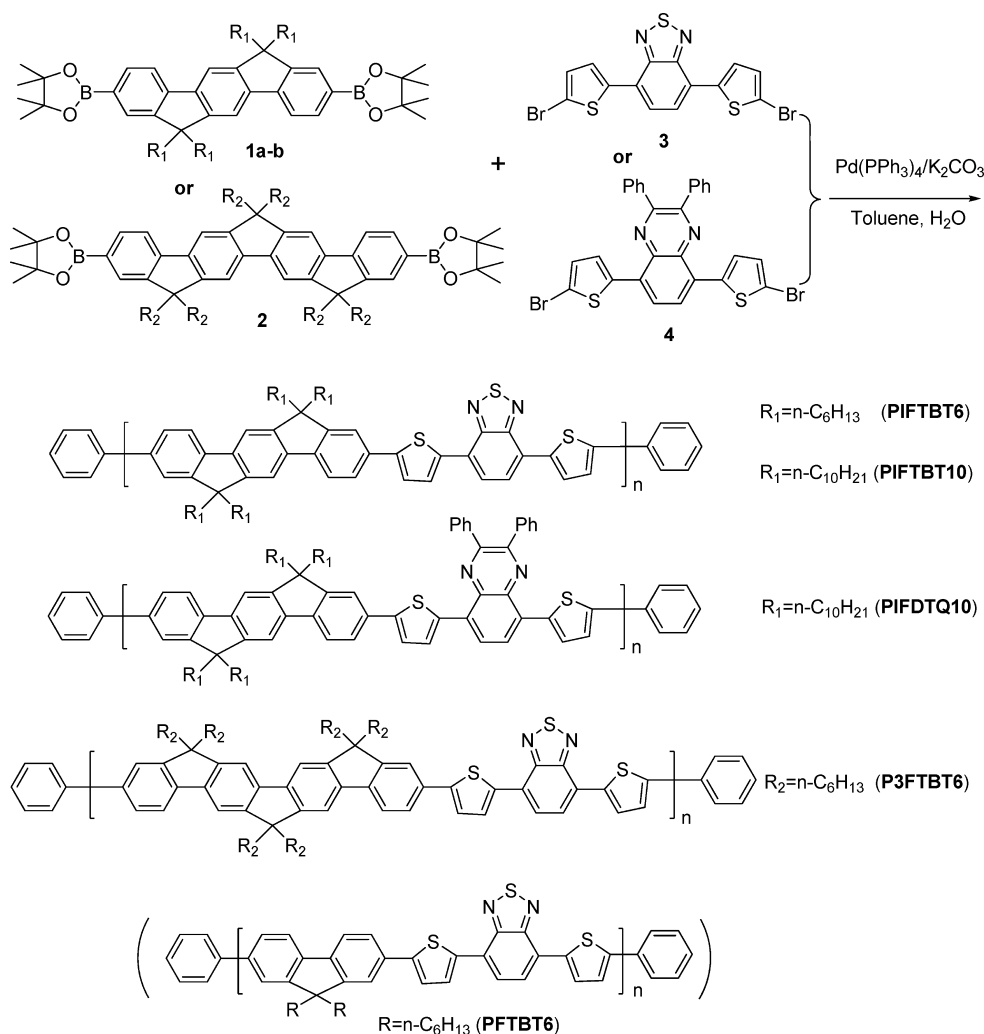
aid of Pd(dppf)Cl₂. In the first step of the synthesis of comonomer **2**, compound **8** was prepared by a 2-fold Suzuki coupling reaction between 2,7-bis(4,4,5,5-tetramethyl-1,3,2-dioxaborolan-2-yl)-9,9-dihexylfluorene (**7**) and methyl 2-bromobenzoate, using (PPh₃)₄Pd(0) as catalyst in a mixture of toluene and an aqueous solution of K₂CO₃ (2 M). Nucleophilic addition to the carboxylic ester (**8**) by *n*-hexyllithium gave the corresponding tertiary alcohol, and then the resulting tertiary alcohol was converted to compound **9** by a ring-closure reaction in the presence of boron trifluoride etherate, via an intramolecular Friedel−Crafts alkylation. In the third step, compound **9** was selectively brominated at the 2- and 10-positions by copper(II) bromide on an aluminum oxide matrix in carbon tetrachloride. Finally compound **10** was reacted with 4,4,4′,4′,5,5,5′,5′-octamethyl-2,2′-bi(1,3,2-dioxaborolane) using catalytic amounts of Pd(dppf)Cl₂ and potassium acetate in DMF to provide compound **2**. The synthesis of the acceptor comonomers, 4,7-bis(5-bromo-2-thienyl)-2,1,3-benzothiadiazole (**3**) and 5,8-bis(5-bromothiophen-2-yl)-2,3-diphenylquinoxaline (**4**), were prepared according to a literature procedure.[40] For comparison purposes, we also prepared a fluorene-containing copolymer (**PFTBT6**) as shown in Scheme 1. The structures of the polymers were determined with NMR spectroscopy. Gel permeation chromatography (GPC) results showed that these polymers have weight-averaged molecular weights of 21−64 kg/mol with polydispersity indexes (PDI) of 1.8−2.7 (Table 1). These polymers have very good solubility in many organic solvents such as THF, toluene, chloroform, chlorobenzene, etc. due to the four or six alkyl chains flanked on both sides of the oligo-phenylenes. For example, the solubility of the indenofluorene-containing copolymer in chlorobenzene is at least several times higher than its analogous fluorene-containing copolymer with the same side chains, which will make the solution processing of solar cell devices easier.

2.2. Optical Absorption and Photoluminescence. The optical absorption and emission spectra of the four polymer solutions (in chlorobenzene) are shown in Figure 1a. For comparison, the absorption spectrum of **PFTBT6** is also included in Figure 1a. The pure polymer films and the films blended with PC₆₁BM (or PC₇₁BM) are shown in Figure 1b−c. Similar to the fluorene-containing polymer **PFTBT6**, all of the four copolymers exhibited two absorption peaks, a typical feature for donor−acceptor copolymers. As shown in Figure 1a, the absorption peaks around 400 nm originate from the π−π* transition of indenofluorene or ladder-type tetra-*p*-phenylene units, while the absorption

(40) (a) Hou, Q.; Xu, Y.; Yang, W.; Yuan, M.; Peng, J.; Cao, Y. *J. Mater. Chem.* **2002**, *12*, 2887–2892. (b) Tsami, A.; Bunnagel, T. W.; Farrell, T.; Scharber, M.; Choulis, S. A.; Brabec, C. J.; Scherf, U. *J. Mater. Chem.* **2007**, *17*, 1353–1355.

Scheme 2. Synthesis of Comonomers **1a**−**b** and **2**
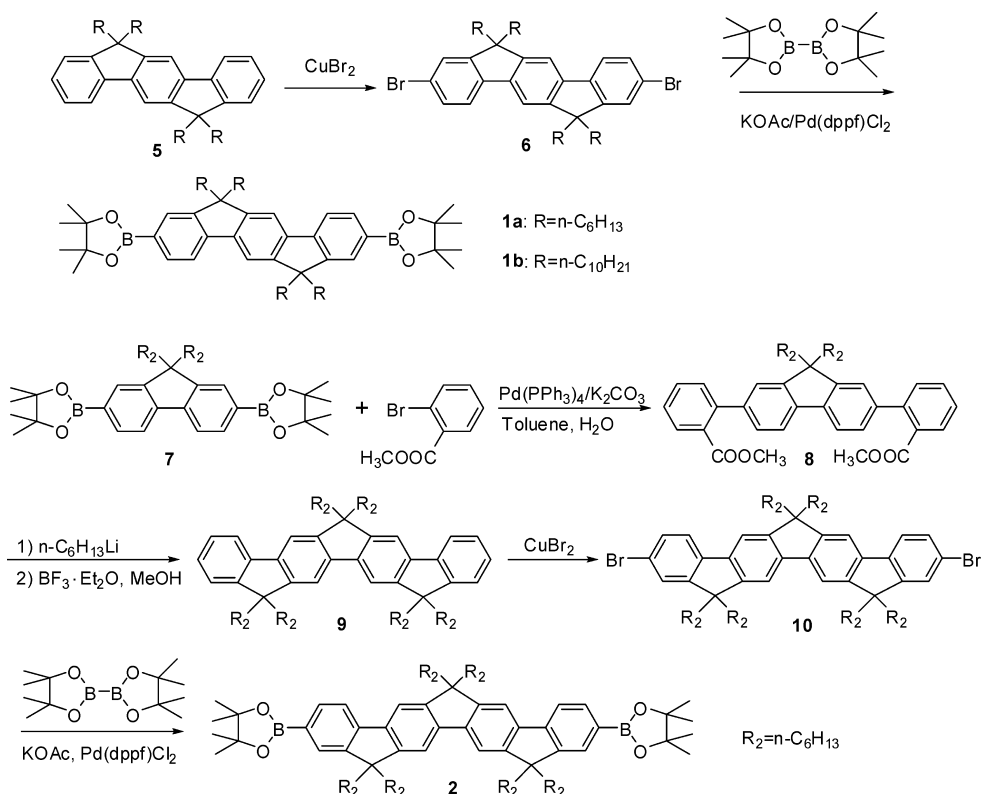
Table 1. Molecular Weight and Optical Absorption of Polymers in Solution and Solid State[a]

polymers	M_n (kg/mol)	M_w (kg/mol)	PDI	absorption		emission		E_g^{opt} (eV)[b]
				solution	film	solution	film	
PIFTBT10	26.3	63.5	2.42	402,542	399,543	613	618	1.97
PIFDTQ10	7.8	21.0	2.65	400,525	395,530	572	671	2.00
PIFTBT6	22.5	45.9	2.03	402,542	399,541	613	618	1.97
P3FTBT6	14.2	24.9	1.75	415,538	408,531	613	618	1.96

[a] Polymers are dissolved in chlorobenzene for absorption and emission spectra of solution samples. [b] Estimated from the onset of the absorption spectra of thin films.

peaks around 540 nm come from the $\pi-\pi^*$ transition of the low band gap acceptor unit. Copolymers **PIFTBT10** and **PIFTBT6** have the same conjugated polymer backbone, but with different lengths of the alkyl chains. In Figure 1a, we can see that their absorption spectra are identical indicating that the alkyl chains will not change the π-conjugated system of polymers. Compared to **PFTBT6**, both peaks of **PIFTBT6** bathochromically shift around 16−19 nm due to the extended π-conjugated system by replacing the fluorene unit with the indenofluorene unit. At the same time, an increased absorption extinction coefficient was found for **PIFTBT6** compared to that for **PFTBT6**. Furthermore, the copolymer **P3FTBT6** shows a more red-shifted linear absorption compared to **PFTBT6** especially for the short wavelength peak, where there is a 32 nm shift from 383 to 415 nm. Besides the bathochromically shifted absorption band, the absorption extinction coefficient for **P3FTBT6** at the short wavelength peak is nearly double compared to **PFTBT6**, which also suggests an improved sunlight absorption ability. The difference between **PIFTBT10** and **PIFDTQ10** is the acceptor unit. **PIFTBT10** shows a red-shifted linear absorption compared to **PIFDTQ10** because the 4,7-dithien-2-yl-2,1,3-benzothiadiazole unit in **PIFTBT10** is a stronger acceptor compared to the 5,8-dithien-2-yl-2,3-diphen-

ylquinoxaline unit in **PIFDTQ10**. The three copolymers with the 4,7-dithien-2-yl-2,1,3-benzothiadiazole repeat unit show almost the same emission spectrum either in solution phase or in the solid film state (Figure S1 in the Supporting Information). **PIFDTQ10** exhibits an ~41 nm hypsochromically shifted emission compared to **PIFTBT10** in a chlorobenzene solution. However, in the solid film state **PIFDTQ10** shows a 53 nm bathochromically shifted emission compared to **PIFTBT10**. This can be attributed to the two phenyl groups in the 5,8-dithien-2-yl-2,3-diphenylquinoxaline unit stretching out from the plane of the polymer backbone in the solution state, whereas in the solid state they may be coplanar with the quinoxaline plane. For some polymers such as P3HT, there is a large red shift of the absorption peak in going from solution phase to solid phase. However, the other three polymers with the 4,7-dithien-2-yl-2,1,3-benzothiadiazole repeat unit show little difference for the absorption and emission spectra in solutions and solid state films. This may be due to the more rigid polymer backbones in these three polymers which prevent their conformal change in the solid state. For polymers **PIFTBT10** and **PIFTBT6**, the optical band gap was found to be 1.97 eV as determined from the onset of the absorption spectra for the solid state films. The optical band gaps of **PIFDTQ10** and **P3FTBT6** were determined to
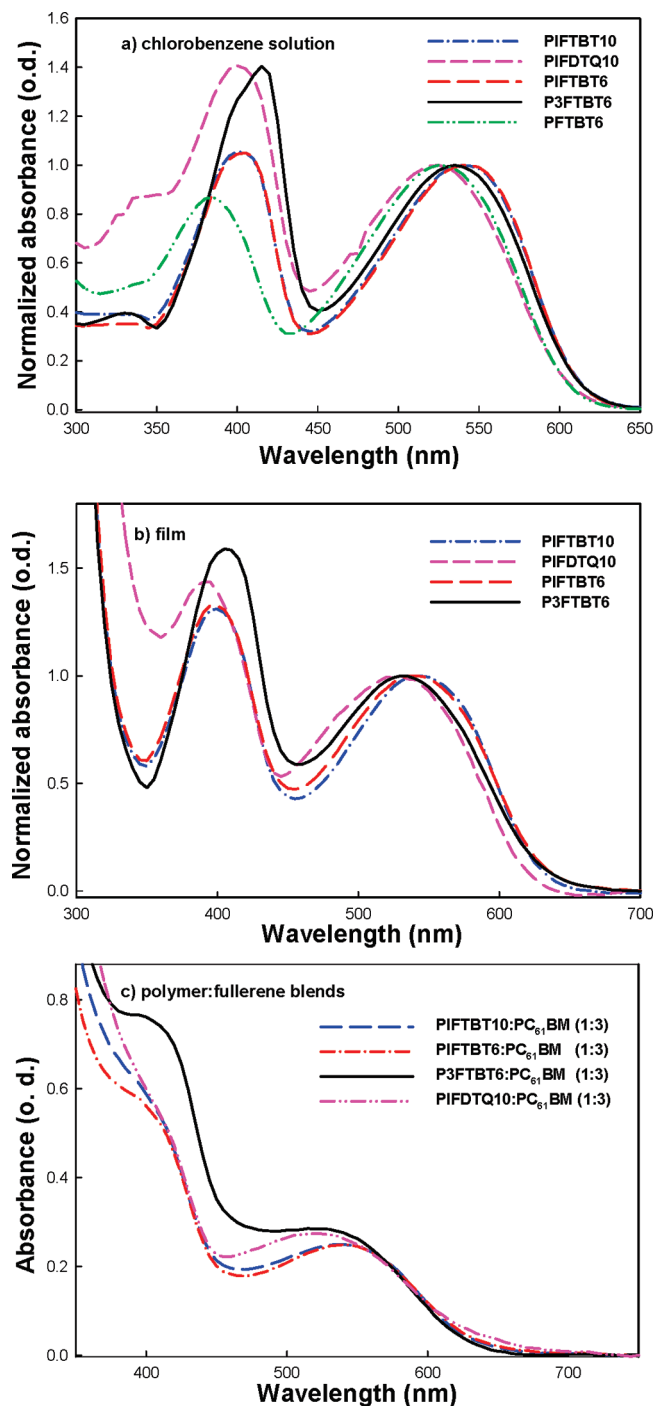
Figure 1. Optical absorption spectra of the targeted polymers in solutions (a), pure polymer films (b), and polymer:fullerene blends.

be 2.00 and 1.96 eV, respectively. Not surprisingly, the optical absorption of the **P3FTBT6**/PC$_{61}$BM blend has an increased absorption extinction coefficient at ~400 nm compared to **PIFTBT10** or **PIFTBT6** blends with PC$_{61}$BM at the same blend ratio (polymer:PC$_{61}$BM = 1:3 by weight).

2.3. Electrochemical Study. For polymers used for solar cells, it is important to know the positions of their HOMO and LUMO levels. Cyclic voltammograms (CV) were performed in a three-electrode cell using platinum electrodes at a scan rate of 50 mV s^{-1} and a Ag/Ag$^+$ (0.1 M of AgNO$_3$ in acetonitrile) reference electrode in an anhydrous and nitrogen-saturated solution of 0.1 M tetrabutylammonium tetrafluoroborate
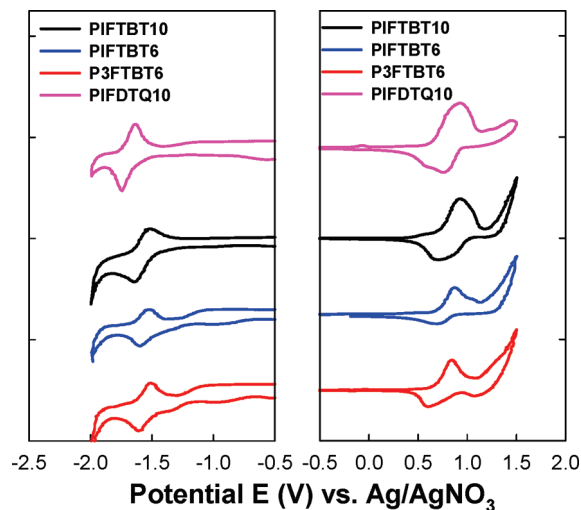

Figure 2. Cyclic voltammetry (CV) of the ladder-type oligo-*p*-phenylene containing copolymers.

(Bu$_4$NBF$_4$) in acetonitrile. Under these conditions, the onset oxidation potential ($E_{1/2}$ ox) of ferrocene was −0.02 V versus Ag/Ag$^+$. The HOMO energy level of polymers was determined from the oxidation onset of the second scan from CV data. It is assumed that the redox potential of Fc/Fc$^+$ has an absolute energy level of −4.80 eV to vacuum.[41] The energy of HOMO and LUMO levels were calculated according to the following equations:

$$E_{HOMO} = -(\phi_{ox} + 4.82) \text{ (eV)} \quad (3)$$

$$E_{LUMO} = -(\phi_{red} + 4.82) \text{ (eV)} \quad (4)$$

where ϕ_{ox} and ϕ_{red} are the onset oxidation potential and the onset reduction potential vs Ag/Ag$^+$ respectively. Cyclic voltammograms of these four polymers (**PIFTBT10**, **PIFDTQ10**, **PIFTBT6**, **P3FTBT6**) are shown in Figure 2. Both reversible reduction and oxidation behaviors were observed for all four polymers, indicating the good structural stability of these polymers in the charged state. For **PIFTBT10**, the onset potentials for oxidation are located around +650 mV versus Ag/AgNO$_3$, which corresponds to a highest occupied molecular orbital of −5.47 eV. The LUMO energy level of **PIFTBT10** is calculated to be ∼ −3.44 eV based on the onset potential for reduction at around −1.37 eV. The electrochemical bandgap of **PIFTBT10** is determined to be 2.03 eV, which is quite close to the band gap (1.97 eV) predicted by solid state optical absorption of the polymer films. The small difference (<0.1 eV) between electrochemical band gap and optical band gap for **PIFTBT10** is similar to some other amorphous polymers,[30] and it could be due to the more rigid polymer backbone for **PIFTBT10** compared to other crystalline polymers (such as P3HT) that usually have larger differences between their electrochemical band gaps and optical band gaps. Using similar methods, the HOMO and LUMO levels and electrochemical band gaps for the other three polymers are calculated and listed in Table 2. The HOMO and LUMO energy levels of the four polymers are in good agreement with the optimal levels for obtaining good performance in photovoltaic cells using PC$_{61}$BM (LUMO: −3.7 eV) or PC$_{71}$BM (LUMO: −3.75 eV) as an

(41) Pommerehne, J.; Vestweber, H.; Guss, W.; Mahrt, R. F.; Bässler, H.; Porsch, M.; Daub, J. *Adv. Mater.* **1995**, *7*, 551–554.

Table 2. Eletrochemical Properties of Polymers[a]

polymers	E_{ox} onset (V)	E_{red} onset (V)	HOMO (eV)	LUMO (eV)	E_g (eV)
PIFTBT10	0.65	−1.38	−5.47	−3.44	2.03
PIFDTQ10	0.63	−1.46	−5.45	−3.36	2.09
PIFTBT6	0.67	−1.36	−5.49	−3.46	2.03
P3FTBT6	0.63	−1.36	−5.45	−3.45	2.00

[a] Measured in a 0.1 M solution of Bu_4NPF_6 in CH_3CN with a Pt electrode and a $Ag/AgNO_3$ reference electrode. In these conditions, the onset oxidation potential ($E_{1/2}$ ox) of ferrocene was −0.02 V versus Ag/Ag^+. It is assumed that the redox potential of Fc/Fc^+ has an absolute energy level of −4.80 eV to vacuum.

acceptor. The deeper lying HOMO levels of these polymers will provide a higher open circuit voltage (V_{oc}) according to the theoretical prediction.[42]

Figure 3 depicts the electron-state-density distribution of the HOMO and LUMO of geometry optimized structures (DFT B3LYP/6-31G) of analogous monomers (a) **PIFTBT6** (**PIFT-BT10**), (b) **P3FTBT6** using the Gaussium 03 program. The results indicate that the electron density of LUMO is mainly localized on the acceptor unit, while the electron density of HOMO is distributed over the entire conjugated molecule (both the acceptor unit and donor unit). Calculated results show that **PIFTBT6** has a HOMO energy level of −5.08 eV, which is somewhat low-lying compared to **P3FTBT6** (−5.03 eV), which has a half-fluorene extended π-conjugation system. These calculated changes for LUMO, HOMO levels and band gaps in going from **PIFTBT6** (**PIFTBT10**) to **P3FTBT6** are also in agreement with the experiment results.

2.4. Field Effect Transistors. Among the requirements for polymer solar cells are an efficient photoinduced charge transfer from the donor molecules (polymers) to acceptors (such as PCBMs) and sufficient transport properties of the polymer blend. It has been demonstrated that PCBMs are good electron transporting materials with sufficient mobility for high performance solar cells.[43] To ensure the hole transporting properties of the polymers, we fabricated field effect transistors (FETs). Top-contact bottom-gate transistors were fabricated under ambient conditions by spin-casting chlorobenzene solutions of the synthesized polymers on the heavily doped Si(100) substrates treated with hexamethyldisilazane (HMDS) or without any surface treatment. Figure 4a−d show the typical current−voltage characteristics of the polymeric FET devices with a channel width and length of approximately 6.5 mm and 270 μm, respectively, where I_d, V_d, V_g represent the source−drain current, source−drain voltage, and gate voltage, respectively. The saturation region mobilities were calculated from the transfer characteristics of the FETs using the slope derived from the square root of the absolute value of the current as a function of gate voltage between −50 and −30 V. The threshold voltages of the polymeric FETs were derived from the onsets of the transfer curves. Device performance data of the four different polymers on two different surface treated substrates are listed in Table 3. From the table, the FETs devices with HMDS treatment gave 4−23-fold higher mobilities compared to those without surface treatment using the same polymer as the semiconducting material. Among the FET devices with HMDS treatment, the motilities for **PIFTBT10**, **PIFDTQ10**, **PIFTBT6**,

and **P3FTBT6** are found to be $(4.2 \pm 0.2) \times 10^{-3}$, $(9.5 \pm 0.7) \times 10^{-4}$, $(1.1 \pm 0.1) \times 10^{-2}$, and $(9.7 \pm 0.3) \times 10^{-3}$ $cm^2/(V\ s)$, in that order. All the devices show clear on/off behavior which will minimize leakage currents. The structure difference in **PIFTBT10** and **PIFTBT6** is the length of side chains. We found a decrease of hole mobility with the longer alkyl chains. It is expected that more bulky side chains may increase the steric hindrance for the intermolecular packing, thus resulting in a decrease in mobility in going from **PIFTBT6** to **PIFTBT10**. Comparing **PIFTBT10** with **PIFDTQ10**, it is found that the mobility of the former is almost 5 times larger than the latter, which may be attributed to the fact that two bulky phenyls in the 5,8-dithien-2-yl-2,3-diphenylquinoxaline repeat unit of **PIFDTQ10** do not lead to a better $\pi-\pi$ packing compared to **PIFTBT10** with the 4,7-dithien-2-yl-2,1,3-benzothiadiazole repeat unit. For the three polymers with the 4,7-dithien-2-yl-2,1,3-benzothiadiazole repeat unit, **PIFTBT6** and **P3FTBT6** show over double the mobility compared to **PIFTBT10**. This could be due to the $\pi-\pi$ packing difference of the polymer backbone as well as the morphological difference induced by the length of the side chains. We performed atomic force microscopy (AFM) surface measurements of these films, and the topographic images are shown in Figure S2. In general, the AFM images of the four polymers show uniform and flat films with roughnesses in the range 0.6−1.0 nm. We did not observe crystalline domains for these polymer films, indicating that all four polymers are amorphous. The films for polymers with longer side chains (**PIFTBT10** and **PIFDTQ10**) show an increased roughness compared to the films for those with short alkyl chains (**PIFTBT6** and **P3FTBT6**).

2.5. Solar Cells. As shown in the inset of Figure 5a, the BHJ solar cells were fabricated with a device structure of ITO/PEDOT:PSS/polymer:fullerene/Cs_2CO_3/Al. After spin-coating a ~40 nm poly(ethylenedioxythiophene polystyrenesulfonate) (PEDOT:PSS) layer on the anode (ITO), the active layers with a thickness of 100−180 nm were spin-coated from a mixed solvent (chlorobenzene:o-dichlorobenzene = 4:1) solution of polymers and fullerenes. Then the cathode, a bilayer of a thin (1.0 nm) Cs_2CO_3 layer covered with 100 nm Al, was thermally evaporated.

Figure 5a−b show the current density−voltage ($J−V$) characteristics of photovoltaic devices based on the four polymer blends under simulated solar light (AM 1.5 G, 100 mW/cm², RT, ambient). Representative characteristics of the solar cells are summarized in Table 4. The cell based on **BisDMO-PFDTBT**/$PC_{61}BM$ serves as a standard reference for the solar cell performance of the four polymers developed in this work.[44] **BisDMO-PFDTBT** is a fluorene containing copolymer exactly the same as **PFTBT6** except the alkyl chains change from n-hexyl to 3,7-dimethyloctyl, which affords better solubility.[44] We did not use **PFTBT6** due to its extremely low solubility in organic solvents. The data in Table 4 show all these polymers showed better performance than the analogous fluorene containing copolymers (**BisDMO-PFDTBT**) except for **PIFTBT6**. Compared to **PIFTBT6**, **PIFTBT10** which contains longer side chains has a higher power conversion efficiency of 2.44% with respect to 0.97% for **PIFTBT6**. This can be due to the solubility differences found for these two polymers which may lead to their phase separation conditions, although the hole mobility of **PIFTBT6** is more than double that of **PIFTBT10**, indicating that the hole mobility of a polymer is not the only parameter

(42) Scharber, M. C.; Wuhlbacher, D.; Koppe, M.; Denk, P.; Waldauf, C.; Heeger, A. J.; Brabec, C. L. *Adv. Mater.* **2006**, *18*, 789−794.

(43) Mihailetchi, V. D.; van Duren, J. K. J.; Blom, P. W. M.; Hummelen, J. C.; Janssen, R. A. J.; Kroon, J. M.; Rispens, M. T.; Verhees, W. J. H.; Wienk, M. M. *Adv. Funct. Mater.* **2003**, *13*, 43−46.

(44) Chen, M.-H.; Hou, J.; Hong, Z.; Yang, G.; Sista, S.; Chen, L.-M.; Yang, Y. *Adv. Mater.* **2009**, *21*, 4238−4242.
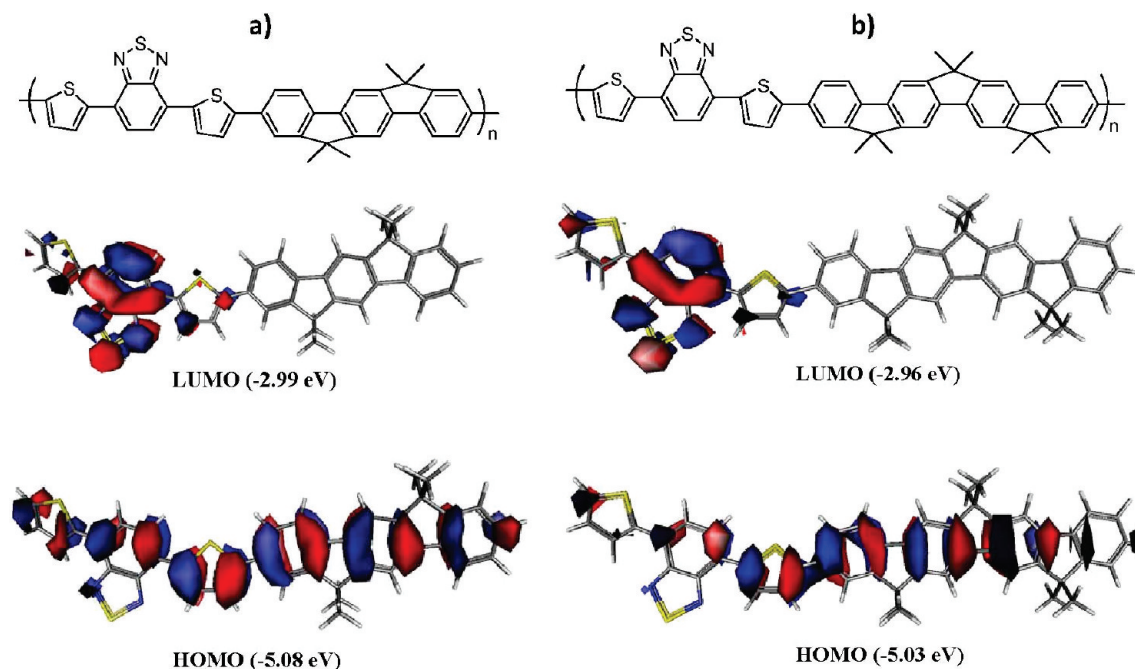
Figure 3. DFT-calculated LUMO and HOMO of the geometry optimized structures of analogous monomers of (a) **PIFTBT6**, **PIFTBT10** and (b) **P3FTBT6**.
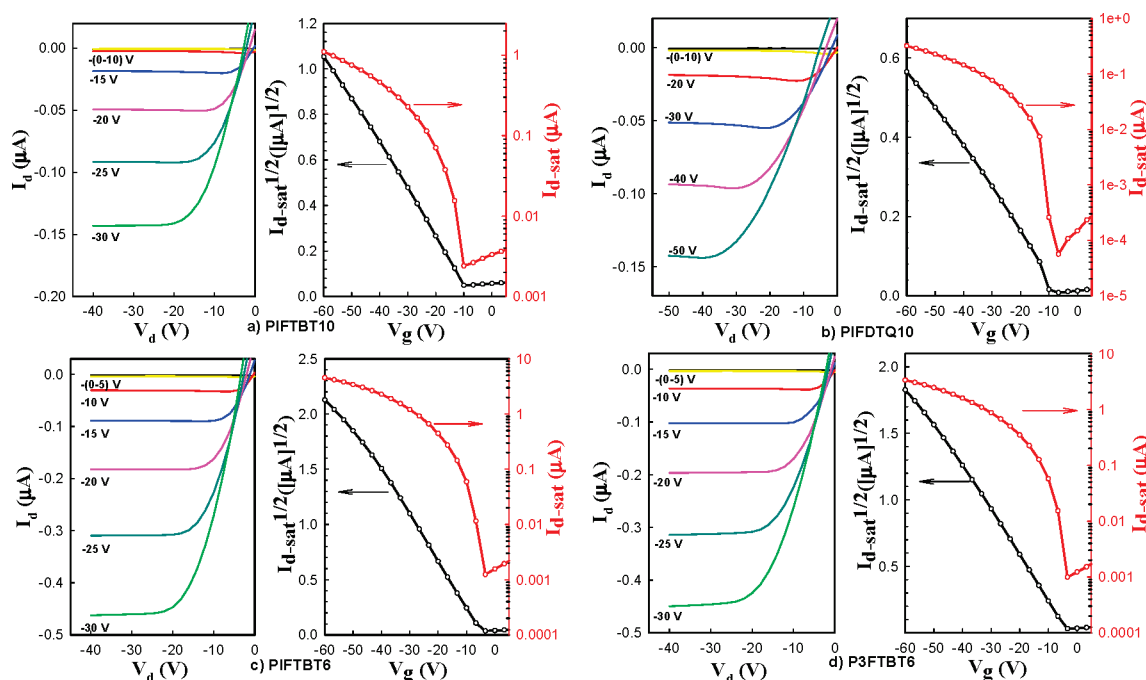

Figure 4. $I_d - V_d$ curves of FET devices as a function of V_g (left), $I_{d\text{-sat}}$, and $I_{d\text{-sat}}^{1/2}$ vs V_g (right) based on spin-cast films for the polymers (a) **PIFTBT10**, (b) **PIFDTQ10**, (c) **PIFTBT6**, and (d) **P3FTBT6**.
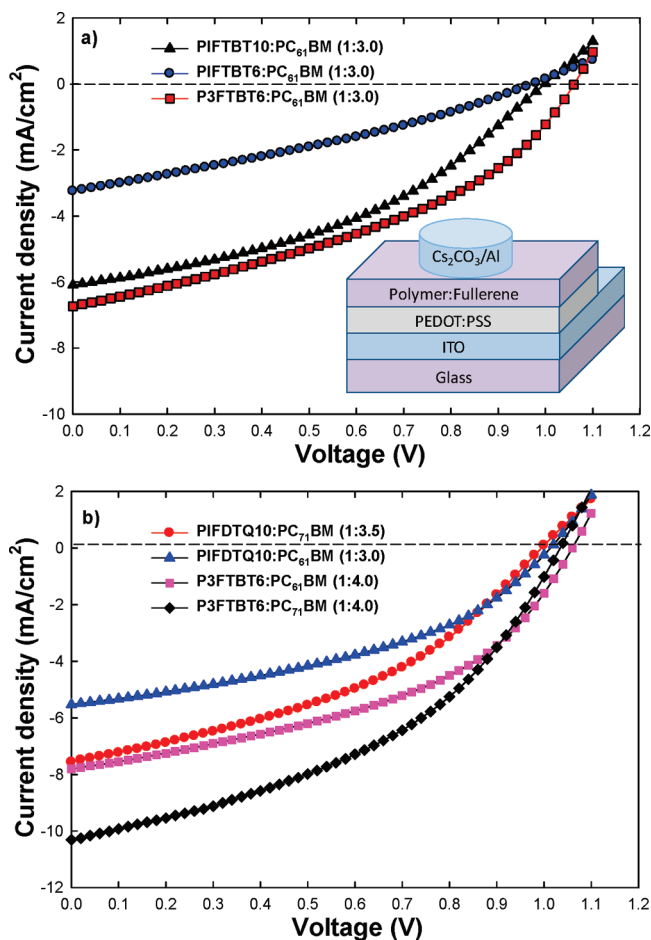
for achieving high performance solar cells. At the same time, the results suggest that the length of the solubilizing group in the indenofluorene unit may play an important role in the solubility and miscibility with fullerene which could lead to a difference in the nanoscale morphology of polymer−fullerene blends. It is well recognized that the performance of solar cells is related to the nanoscale morphology of polymer−fullerene blends influenced by parameters including the solvent, the processing temperature, the solution concentration, the relative ratio in composition between polymer and fullerene, the thermal annealing process, the chemical structure of polymer, etc. Since

we have not yet fully optimized the conditions for the device fabrication of all the polymers, the data shown in Table 4 do not represent the best performance for all four polymers. The comparison here is merely based on one specific device fabrication condition. The different solar cell performances found for **PIFTBT6** and **PIFTBT10** show that the performance of this type of copolymer can be further improved by introducing some possibly better side chains such as branched alkyl chains.

For **PIFDTQ10**, we chose both $PC_{61}BM$ and $PC_{71}BM$ as acceptors in the active layer. **PIFDTQ10** shows a high short-circuit current (J_{sc}) of 7.57 mA/cm², an open-circuit voltage (V_{oc})

Table 3. Mobilities, On−Off Current Ratios, and Threshold Voltages of Polymers Based OFETs Measured in Air[a]

polymers	substrate treatment	μ (cm^2 V^{-1} s^{-1})	V_{th} (V)	on/off
PIFTBT10	none	$(1.8 \pm 0.4) \times 10^{-4}$	7−25	10^3
PIFTBT10	HMDS	$(4.2 \pm 0.2) \times 10^{-3}$	6−12	10^3
PIFDTQ10	none	$(2.3 \pm 0.2) \times 10^{-4}$	3−13	10^3
PIFDTQ10	HMDS	$(9.5 \pm 0.7) \times 10^{-4}$	3−8	10^3
PIFTBT6	none	$(1.1 \pm 0.1) \times 10^{-3}$	3−10	10^3
PIFTBT6	HMDS	$(1.1 \pm 0.1) \times 10^{-2}$	5−8	10^3
P3FTBT6	none	$(6.1 \pm 0.5) \times 10^{-4}$	1−13	10^3
P3FTBT6	HMDS	$(9.7 \pm 0.3) \times 10^{-3}$	4−7	10^3

[a] Threshold voltage (V_{th}). HMDS: hexamethyldisilazane.

Table 4. Summary of Device Parameters of the ITO/PEDOT:PSS/Polymer:Fullerene/Cs$_2$CO$_3$/Al Devices[a]

polymers	blend ratio with PC$_{61}$BM	V_{oc} (V)	J_{sc} (mA cm^{-2})	fill factors	efficiencies
PIFDTQ10	1:3.0	1.01	5.53	0.42	2.32
PIFDTQ10	1:3.5[b]	1.00	7.57	0.40	3.04
PIFTBT10	1:3.0	1.00	6.10	0.40	2.44
PIFTBT6	1:3.0	0.98	3.25	0.31	0.97
P3FTBT6	1:3.0	1.06	6.73	0.39	2.81
P3FTBT6	1:4.0	1.06	7.80	0.44	3.67
P3FTBT6	1:4.0[b]	1.04	10.3	0.42	4.50
BisDMO-PFDTBT	1:3.0	0.94	4.45	0.42	1.75

[a] Short-circuit current density (J_{sc}), open-circuit voltage (V_{oc}). [b] Blend with PC$_{71}$BM.

Figure 5. (a) Current density−voltage (J−V) characteristics of PV devices based on **PIFTBT10** (or **PIFTBT6**, **P3FTBT6**):PC$_{61}$BM polymer blends under simulated solar light (AM 1.5 G, 100 mW/cm^2, RT, ambient). (b) Current density−voltage (J−V) characteristics of PV devices based on **PIFDTQ10**(**P3FTBT6**):PC$_{71}$BM(PC$_{61}$BM) polymer blends under simulated solar light (AM 1.5 G, 100 mW/cm^2, RT, ambient). Inset is the schematic device structure for the polymer/fullerene bulk heterojunction solar cells.

of 1.00 V, a fill factor of 0.40, and a PCE of 3.04% when it was blended with PC$_{71}$BM at a ratio of (1:3.5 by weight). In comparison, when it is blended with PC$_{61}$BM, a moderate J_{sc} of 5.53 mA/cm^2, a V_{oc} of 1.01 V, and a fill factor of 0.42 are achieved with the resulting power conversion efficiency of 2.32%. The increased efficiency for **PIFDTQ10**:PC$_{71}$BM can be attributed to the increasing optical absorption of the polymer blends, which leads to the increased short-circuit current.[45] **P3FTBT6** and **PIFTBT6** have the same side chains, but **P3FTBT6** has an increased π-conjugation length (one-half the length of a fluorene). **P3FTBT6**:PC$_{61}$BM blends show a much

higher power conversion efficiency of 2.81% in comparison to 0.97% for **PIFTBT6**:PC$_{61}$BM with the same device configuration. Surprisingly, the **P3FTBT6**:PC$_{61}$BM blends show a higher V_{oc} of 1.06 V compared to 0.98 V for **PIFTBT6**:PC$_{61}$BM, although the HOMO level of **P3FTBT6** is in fact slightly higher than that for **PIFTBT6**. We also fabricated **P3FTBT6**:PC$_{61}$BM solar cell devices with a higher fullerene blend ratio (1:4), and the results are shown in Table 4. Although no extensive optimization work has been carried out, an outstanding short-circuit current (J_{sc}) of 7.80 mA/cm^2 and a high open-circuit voltage (V_{oc}) of 1.06 V are reached for the **P3FTBT6** blends with PC$_{61}$BM (1:4). The best results were a power conversion efficiency of 3.67% and a fill factor of 0.44. Furthermore, when PC$_{71}$BM was chosen as an electron acceptor material (**P3FTBT6**: PC$_{71}$BM = 1:4) for the solar cells, a short-circuit current (J_{sc}) of 10.3 mA/cm^2 and a high open-circuit voltage (V_{oc}) of 1.04 V are achieved yielding an outstanding power conversion efficiency of 4.5%. As shown in Figure 5, devices fabricated from both blend ratios of **P3FTBT6** to PC$_{61}$BM showed a high open circuit voltage of 1.06 V. This observation indicated that V_{oc} is correlated not only to the difference between the HOMO of the donor and the LUMO of the acceptor but also to the molecular structural attributes of a polymer such as rigidity and planarity. The open circuit voltage of 1.06 V is higher than analogous donor−acceptor copolymers using fluorene (0.94 V) as the donor as shown in Table 4. It is also higher than other donor−acceptor copolymers using carbazoles (0.88 V) as the donor unit[30,31] and much higher than the P3HT/PC$_{61}$BM system (0.60 V) with similar short circuit currents.[7] We should point out that our devices are fabricated and tested in an ambient environment without any encapsulation. We realize that the fill factors of our devices are not high (0.44), and the photocurrents in reverse bias show a mild field dependence due to the field-dependent exciton dissociation rate, and thus reduced fill factors. These low fill factors can also be attributed to the unbalanced transport of charge carriers and the relatively thick active polymer-fullerene layers (>100 nm) and high trap densities in the devices under ambient environment. An optical spacer or a hole blocker such as titanium oxide (TiO$_x$) between the active polymer−fullerene layer can be used to increase the fill factors of solar cell devices.[31] Therefore with all these considerations, there should be opportunities to further optimize the solar cell performance by fabricating and testing devices in the glovebox, excluding oxygen and water to reduce traps, by engineering the active layer−electrode interface, and by carefully tracing sources of parasitic external resistances throughout our device structures.

(45) Wienk, M. M.; Kroon, J. M.; Verhees, W. J. H.; Knol, J.; Hummelen, J. C.; van Hal, P. A.; Janssen, R. A. J. *Angew. Chem., Int. Ed.* **2003**, *42*, 3371–3375.
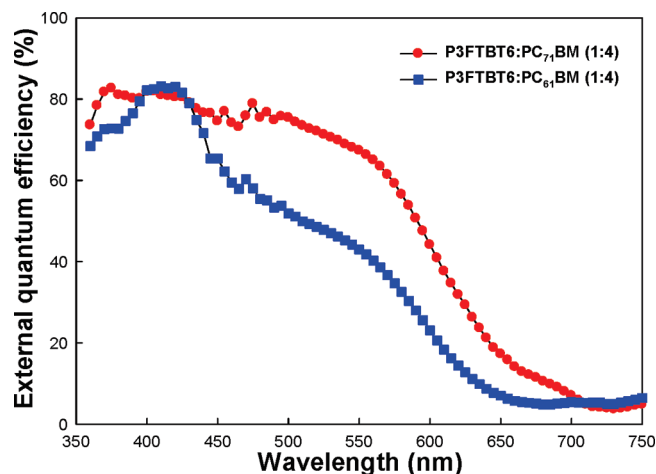
Figure 6. External quantum efficiencies of photovoltaic cells calculated from the photocurrents under short-circuit conditions based on **P3FTBT6**:$PC_{61}BM$ (blue) and **P3FTBT6**:$PC_{71}BM$ (red).

The external quantum efficiencies (EQE) as a function of wavelength of the photovoltaic cells based on **P3FTBT6**:$PC_{61}BM$ (blue) and **P3FTBT6**:$PC_{71}BM$ (red) are shown in Figure 6. As shown in the figure, the **P3FTBT6**:$PC_{61}BM$ blend shows an EQE value of 0.82 at ∼410 nm. This EQE peak is very close to the absorption peak (408 nm) of the copolymer, which indicates that the photovoltaic conversion arises from the absorption of the copolymer. For the device based on **P3FTBT6**:$PC_{71}BM$, increased EQE values are observed in the range 450−700 nm, which is due to the increased absorption by $PC_{71}BM$ compared to $PC_{61}BM$. The broader profile and higher values of EQE found for the **P3FTBT6**:$PC_{71}BM$ are consistent with the higher J_{sc} measured in solar cells compared to **P3FTBT6**:$PC_{61}BM$.

The morphological requirement for the active layer in high performance PSCs is nanoscale phase separation, which enables a large interface area for exciton dissociation and, in the mean time, a continuous percolating path for hole and electron transport to the corresponding electrodes. In this work, AFM was used to characterize the morphology of the polymer:PCBMs blends. These AFM topography and phase images are shown in Figures 7 and 8. As shown in Figure 7a and b, the AFM measurement demonstrates the nanoscale (>10 nm) phase separation for **PIFTBT10**:$PC_{61}BM$ and **PIFDTQ10**:$PC_{61}BM$ blends, which result in ∼100 nm sized clusters for the blended films. Measurements on polymers:$PC_{61}BM$ with different blend ratios reveal that the dark areas are attributed to $PC_{61}BM$ domains. Phase separation with the formation of $PC_{61}BM$-rich domains facilitates an improved charge transport and carrier collection efficiency, which results in a reduction of recombination losses and an increase in short-circuit current density. From Figures 7 and 8, one may find that the length of side chains has some impact on the roughness as well as the phase separation size. In general, longer alkyl chains (decyl) lead to an increased roughness as well as enlarged domain sizes. For **PIFTBT10** and **PIFDTQ10** with the 10-carbon alkyl chains, the roughness of the blend films with $PC_{61}BM$ is in the range 3.5−4.0 nm, whereas, for **PIFTBT6** and **P3FTBT6** with 6-carbon alkyl chains, the roughness is in the range 1.3−1.5 nm. In Figure 7a, **PIFTBT10** is homogeneously distributed in the matrix with a domain size of ∼20 nm in comparison to a domain size of 10 nm for **PIFTBT6** in Figure 7. As shown in Figure 8a and b, two different blend ratios of **P3FTBT6** to $PC_{61}BM$ led to
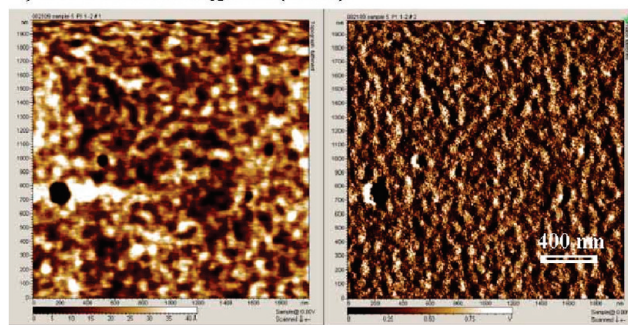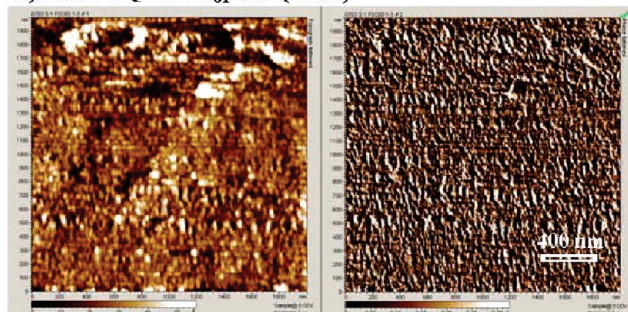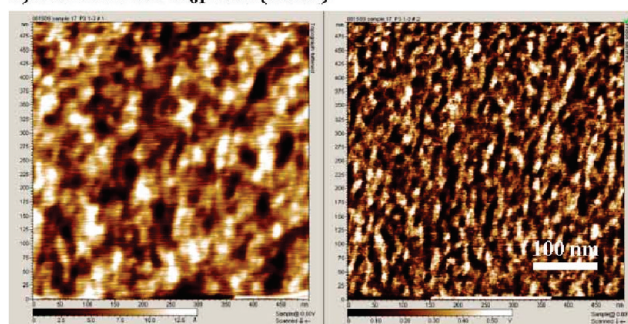

Figure 7. AFM topography images of **PIFTBT10**:$PC_{61}BM$ (a), **PIFDTQ10**:$PC_{61}BM$ (b), and **PIFTBT6**:$PC_{61}BM$ (c) films spin-cast from a mixture of chlorobenzene and *o*-dichlorobenzene (left) and surface phase images of the films (right).

different domain sizes of the films as well as the shapes of the interpenetrated network. These morphology differences are also reflected by the photovoltaic behavior of the **P3FTBT6**:$PC_{61}BM$ films. In Figure 8b, for the **P3FTBT6**/$PC_{61}BM$ blended film, the bright patterns of **P3FTBT6** domains show an interpenetrating network which enables a large interface area for exciton dissociation as well as a continuous percolated path for hole and electron transport to the corresponding electrodes. This may be responsible for the improved performance of the device from 2.81% (1:3) to 3.67% (1:4). Figure 8c shows the AFM topography and phase images of **P3FTBT6**:$PC_{71}BM$. When the electron acceptor material changed from $PC_{61}BM$ to $PC_{71}BM$, an increased roughness of ∼2.5 nm is observed compared to 1.5 nm for **P3FTBT6**:$PC_{61}BM$, which could be due to the increased molecular size of $PC_{71}BM$. However, pronounced nanoscale phase separation (>10 nm) is still seen for the **P3FTBT6**:$PC_{71}BM$ blend.

3. Conclusions

In conclusion, we have successfully synthesized a series of donor−acceptor ladder-type oligo-*p*-phenylene-containing co-
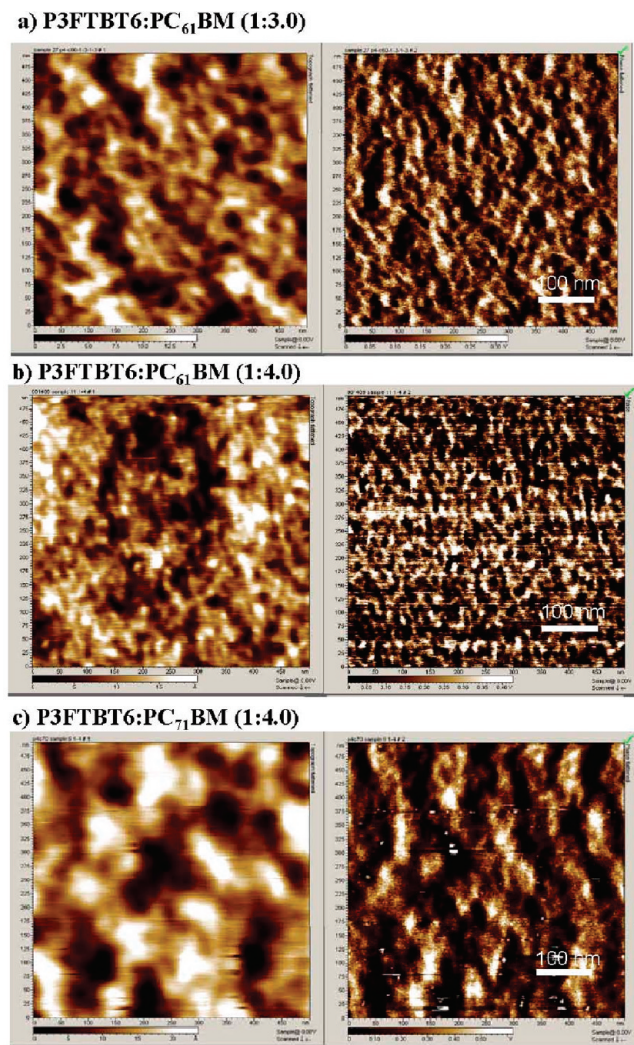
a) P3FTBT6:PC₆₁BM (1:3.0)

b) P3FTBT6:PC₆₁BM (1:4.0)

c) P3FTBT6:PC₇₁BM (1:4.0)

Figure 8. AFM topography images of **P3FTBT6**:$PC_{61}BM$ films with two different blend ratios and **P3FTBT6**:$PC_{71}BM$ films spin-cast from a mixture of chlorobenzene and *o*-dichlorobenzene (left) and surface phase images of the films (right).

polymers, **PIFDTQ10**, **PIFTBT10**, **PIFTBT6**, and **P3FTBT6**. Incorporation of indenofluorene or ladder-type tetra-*p*-phenylene, an electron donating building block to the polymer backbone, leads to an enhanced and bathochromically shifted absorption band compared to the fluorene containing analogous copolymers. At the same time, the HOMO energy levels of these polymers were kept low, which results in a more than 60% increase in operating voltage compared to P3HT and many low band gap polymers. Without extended optimization, a high power conversion efficiency of 3.67% and a high V_{oc} of 1.06 V were achieved from a **P3FTBT6**:$PC_{61}BM$ (1:4) blend under the ambient environment, which is superior to that of the analogous fluorene containing copolymer (**BisDMO-PFDTBT**) cell (1.75%) under the same experimental conditions. A high power conversion efficiency of 4.50% and a high open-circuit voltage of 1.04 V were also achieved from a polymer solar cell device with an active layer containing 20 wt % **P3FTBT6** and 80 wt % $PC_{71}BM$. The absorption range of this type of donor−acceptor copolymer can be further bathochromically tuned to better match the solar spectrum by using a still stronger acceptor. These results show that ladder-type oligo-*p*-phenylene containing

copolymers are promising candidates for achieving BHJ solar cells with high conversion efficiencies and high open circuit voltages.

4. Experimental Section

Reagents were purchased from Aldrich Inc. and Lancaster Synthesis Ltd. and used without further purification unless otherwise stated. 6,6′,12,12′-Tetradecyl-6,12-dihydroindeno[1,2*b*]fluorene, 4,7-bis(5-bromo-2-thienyl)-2,1,3-benzothiadiazole, 5,8-bis(5-bromothiophen-2-yl)-2,3-diphenylquinoxaline, and 2,8-dibromo-6,6′,12,12′-tetradecyl-6,12-dihydroindeno-[1,2*b*]fluorene were prepared according to the literature procedures.[33,35,40] Column chromatography was conducted with silica gel 60 (400 mesh). ¹H NMR spectra were recorded at either 300 or 400 MHz. Absorption and fluorescence spectra were acquired using a spectrophotometer (Cary 50 UV/vis) and a Jobin-Yvon Fluolog FL-3.11 spectrofluorometer, respectively.

2,8-Dibromo-6,6′,12,12′-tetradecyl-6,12-dihydroindeno-[1,2*b*]fluorene (6b). To a solution of 6,6′,12,12′-tetradecyl-6,12-dihydroindeno[1,2*b*]fluorene (**5b**) (4.0 g; 4.9 mmol) in CCl_4 (100 mL) was added copper(II) bromide (5.6 g) on aluminum oxide (11.2 g). After the reaction mixture had been refluxed for 24 h, it was filtered, and the organic filtrate was washed with water and dried over magnesium sulfate. Removing the solvent afforded the crude product, which was purified by column chromatography on silica gel, eluting with petroleum ether. The title compound **6b** (4.5 g, 90%) was collected as a yellow crystalline solid. ¹H NMR (300 MHz, $CDCl_3$, δ): 7.58 (d, $J = 8.4$ Hz, 2H), 7.54 (s, 2H), 7.47−7.44 (m, 4H), 1.98 (t, $J = 8.1$ Hz, 8H), 1.55−1.03 (m, 56H), 0.89−0.83 (m, 12 H), 0.60 (bs, 8H); HRMS calcd for $C_{60}H_{92}Br_2$, 970.5566; found, 970.5552.

2,2′-(6,6,12,12-Tetradecyl-6,12-dihydroindeno[1,2*b*]fluorene-2,8-diyl)bis(4,4,5,5-tetramethyl-1,3,2-dioxaborolane) (1b). 2,8-Dibromo-6,6′,12,12′-tetradecyl-6,12-dihydroindeno-[1,2*b*]fluorene **6b** (4.5 g, 4.6 mmol), bis(pinacolato)diboron (4.6 g, 18.1 mmol), $PdCl_2$(dppf) (250 mg, 0.3 mmol), and KOAc (3.0 g, 30 mmol) in degassed DMF (50 mL) were stirred at 65 °C overnight. The reaction was quenched by adding water, and the resulting mixture was washed with petroleum ether (100 mL × 3). The organic layers were washed with brine, dried over Na_2SO_4, and concentrated in vacuo to a white solid. The solid was purified by silica gel chromatography by 20% methylene chloride in hexane to give the desired compound as a white solid (3.75 g, 78%). ¹H NMR(400 MHz, $CHCl_3$, δ): 7.77 (d, $J = 8.4$ Hz, 2H), 7.74 (d, $J = 5.6$ Hz, 2H), 7.63 (s, 2H), 2.10−1.90 (m, 8H), 1.40 (s, 24 H), 1.20−1.00 (m, 56H), 0.81 (t, $J = 7.2$ Hz, 12H), 0.56 (bs, 8H). HRMS calcd for $C_{72}H_{116}B_2O_4$, 1066.9060; found, 1066.9078.

2,2′-(6,6,12,12-Tetrahexyl-6,12-dihydroindeno[1,2*b*]fluorene-2,8-diyl)bis(4,4,5,5-tetramethyl-1,3,2-dioxaborolane) (1a). Compound **1a** was prepared as a white crystalline solid according to the same procedure as that for compound **1b**. Yield: 58%. ¹H NMR (400 MHz, $CHCl_3$, δ): 7.79 (d, $J = 8.4$ Hz, 2H), 7.75 (d, $J = 5.4$ Hz, 4H), 7.63 (s, 2H), 2.07−1.99 (m, 8H), 1.40 (s, 24H), 1.08−1.00 (m, 24H), 0.71(t, $J = 6.6$ Hz, 12H), 0.61 (bs, 8H). HRMS calcd for $C_{56}H_{84}B_2O_4$, 842.6556; found, 842.6559.

Synthesis of Compound 2. Compound **2** was prepared according to the same procedure as that for compound **1b** from compound **10**.[35] Yield: 48%. ¹H NMR (400 MHz, $CHCl_3$, δ): 7.78 (d, $J = 8.4$ Hz, 2H), 7.74 (d, $J = 4.8$ Hz, 4H), 7.65 (s, 2H), 7.63 (s, 2H), 2.10−2.03 (m, 12H), 1.41 (s, 24 H), 1.03 (bs, 40H), 0.72−0.66 (m, 30H). HRMS calcd for $C_{75}H_{112}B_2O_4$, 1098.8747; found, 1098.8769.

Synthesis of PIFDTQ10. 2,2′-(6,6,12,12-Tetradecyl-6,12-dihydroindeno[1,2*b*]fluorene-2,8-diyl)bis(4,4,5,5-tetramethyl-1,3,2-dioxaborolane) (0.56 g, 0.53 mmol), 5,8-bis(5-bromo-2-thienyl)-2,3-diphenylquinoxaline (0.317 g, 0.53 mmol), and 20 mL of K_2CO_3 solution (2 M in H_2O) were added into a three-neck flask containing 50 mL of toluene. The flask was connected to a reflux condenser

and filled with nitrogen. After bubbling the toluene solution for 30 min, 50 mg of Pd(PPh$_3$)$_4$ (ca. 5 mol %) were added. The degassed reaction mixture was stirred under nitrogen at 95 °C for 2 days. Workup of the reaction mixture and isolation of the polymer occurred by extraction with chloroform; washing of the combined organic extracts with 1 M HCl, a sat. aqueous NaHCO$_3$ solution, and water; and drying over MgSO$_4$. Then this organic extract was filtered through a short florisil column. After partial evaporation of the solvent, the concentrated solution was precipitated into methanol, and the solid was collected by filtration and extracted in a Soxhlet setup with methanol for 24 h and then with hexane for another 24 h. The insoluble remainders were redissolved in chloroform and precipitated into methanol. After filtration and drying in vacuo at 50 °C overnight, 0.30 g of the polymers was obtained (45% yield). ^{1}H NMR (400 MHz, CDCl$_3$, δ): 8.24 (s, 2H), 7.96−7.47 (m, 22H), 2.11 (bs, 8H), 1.20−1.00 (m, 56H), 0.84−0.77 (m, 20H). GPC: M_n = 7.8 kg/mol, M_w = 21 kg/mol, PDI = 2.65.

Synthesis of PIFTBT10. PIFTBT10 was prepared according to the same procedure as that for **PIFDTQ10**. 71% yield, ^{1}H NMR (300 MHz, CDCl$_3$, δ): 8.18 (s, 2H), 7.97 (s, 2H), 7.79−7.53 (m, 10H), 2.10 (bs, 8H), 1.21−1.00 (m, 56H), 0.83−0.73 (m, 20H). GPC M_n = 26.3 kg/mol, M_w = 63.5 kg/mol, PDI = 2.42.

Synthesis of PIFTBT6. PIFTBT6 was prepared according to the same procedure as that for **PIFDTQ10**. 31% yield, ^{1}H NMR (300 MHz, CDCl$_3$, δ): 8.18 (s, 2H), 7.98 (s, 2H), 7.80−7.54 (m, 10H), 2.11 (bs, 8H), 1.17 (bs, 24H), 0.77−0.68 (m, 20H). GPC M_n = 22.5 kg/mol, M_w = 45.9 kg/mol, PDI = 2.03.

Synthesis of P3FTBT6. P3FTBT6 was prepared according to the same procedure as that for **PIFDTQ10**; 43% yield; ^{1}H NMR (300 MHz, CDCl$_3$, δ): 8.19 (s, 2H), 7.98 (s, 2H), 7.80−7.53 (m, 12H), 2.11 (bs, 12H), 1.10 (bs, 36H), 0.75−0.70 (m, 30H). GPC M_n = 14.2 kg/mol, M_w = 24.9 kg/mol, PDI = 1.75.

Computational Methods. All of the DFT calculations were performed with the Gaussian 03 program package (Gaussian, Inc.). The structures shown in Figure 3 were fully optimized without any symmetry restrictions at the B3LYP level. A split-valence plus polarization basis set, 6-31G(d), was used. The DFT/B3LYP/6-31G(d)-optimized structures for the model compounds were used for electronic-structure analysis. HOMO and LUMO isosurfaces shown in Figure 3 were plotted using the Gabedit software (http://gabedit.sourceforge.net).

Field-Effect Transistors. Top contact FETs of copolymers were fabricated on hexamethyldisilazane (HMDS)-treated or untreated SiO$_2$/Si substrates. The semiconducting films were deposited by spin-casting pure polymers (~7 mg/mL in chlorobenzene) at 1500 rpm on the substrates. Gold top contact source and drain electrodes of ~50 nm thickness were vapor deposited through a shadow mask. The channel widths and lengths were ~6.5 mm and 270 μm, respectively. Devices were measured in air using an Agilent 4155C semiconductor parameter analyzer with the ICS lite software.

Solar Cell Fabrication. The indium tin oxide (ITO)-covered glass substrates were cleaned by ultrasonification sequentially in detergent, water, acetone, and isopropyl alcohol for 30 min each and then dried in an oven at 90 °C overnight. A thin layer (~40 nm) of poly(3,4-ethylenedioxythiophene)/poly(styrene sulfonic acid) PEDOT/PSS (Baytron P Al 4083) was spin-coated onto the ITO surface, which was pretreated by oxygen plasma for 5 min. The substrates were baked at 120 °C for 2 h. An active layer (150−180 nm) was fabricated in the ambient by spin-casting (800 rpm) a blend of polymer:PC$_{61}$BM/polymer:PC$_{71}$BM (purchased from Nano C) in a 1:3 (or 1:3.5) w/w ratio on the ITO/PEDOT:PSS substrates without further special treatment. For optimization of **P3FTBT6**, an active layer of (100−110 nm) was fabricated in the ambient by

spin-casting (1500 rpm) a blend of **P3FTBT6**:PC$_{61}$BM or **P3FTBT6**:PC$_{71}$BM in a 1:4 w/w ratio on the ITO/PEDOT:PSS substrates. Then the devices were kept at room temperature for 24 h. Then, the cathode, a bilayer of a thin (1.0 nm) Cs$_2$CO$_3$ layer covered with 100 nm Al, was thermally evaporated. The thermal evaporation of Cs$_2$CO$_3$ and Al was done under a shadow mask. The active area of the devices was fixed at 0.07 cm^2. As shown in the inset of Figure 5, an island-type cathode design was chosen to exclude any excess photocurrent generated from the parasitic solar cell structure, where the conductive PEDOT layer can act as an effective anode.[46] Four polymers and PC$_{61}$BM (or PC$_{71}$BM) were dissolved together in a mixture of chorobenzene and *o*-dichlorobenzene (4:1, v/v) to give an overall 20 mg/mL solution. **PIFDTQ10** and PC$_{71}$BM were dissolved together in a mixture of chorobenzene and *o*-dichlorobenzene (4:1, v/v) to give an overall 28 mg/mL solution.

Device Characterization. Device characterization in ambient environment was performed under AM 1.5G irradiation (100 mW/cm^2) on an Oriel Xenon solar simulator. The solar cell devices were illuminated through their ITO sides. The current density−voltage curves were measured in air by an Agilent 4155C semiconductor parameter analyzer with the ICS lite software. Since there are some deviations in the spectral output of the solar simulator with respect to the standard AM1.5 spectrum, the J_{sc} values for the solar cell devices were corrected by introducing a mismatch factor as shown in eq 5:

$$J_{sc} = J_{sc}(\text{measured}) \times m \qquad (5)$$

where m is the spectral mismatch factor calibrated using an NREL-calibrated PV-measurement mono-Si solar cell. For all short circuit currents and power conversion efficiencies we used a mismatch factor of 0.87. External quantum efficiencies (EQEs) ware calculated from the photocurrents under short-circuit conditions. The solar cell device was illuminated through its ITO side with a 100 W Xe lamp (PhotoMax) coupled to a 1/4 m monochromator (Oriel Cornerstone). Incident irradiances were measured using an optometer (Graesby Optronics S370 with a United Detector Technology silicon detector), and photocurrents were measured using an electrometer (Keithley 617).

Atomic Force Microscopy. AFM was performed in tapping mode using a Digital Instruments microscope (Molecular Imaging PicoPlus). Films for AFM were prepared on PEDOT:PSS-coated ITO substrates prepared in identical fashion to those prepared for device fabrication. The average roughnesses of films were calculated from AFM topography images of scanned areas using the Gwyddion analysis tool (downloadable from http://gwyddion.net).

Supporting Information Available: Emission spectra and AFM topography images. This material is available free of charge via the Internet at http://pubs.acs.org.

JA909111P

(46) Kim, M.-S.; Kang, M.-G.; Guo, L. J.; Kim, J. *Appl. Phys. Lett.* **2008**, *92*, 133301/1–133301/3.